J. theor. Biol. (2002) **218,** 155–173
doi:10.1006/yjtbi.3064, available online at http://www.idealibrary.com on IDEAL®

A Cellular Tensegrity Model to Analyse the Structural Viscoelasticity of the Cytoskeleton

PATRICK CAÑADAS*†‡, VALERIE M. LAURENT‡, CHRISTIAN ODDOU†, DANIEL ISABEY‡ AND SYLVIE WENDLING†

†*B2OA CNRS UMR*-7052 *Faculté des Sciences et Technologie*, *Université Paris* 12/*Val-de-Marne*, 61 *avenue du Général de Gaulle*, 94 010 *Créteil Cedex*, *France and* ‡*INSERM UMR* 492, *Faculté de Médecine*, *Université Paris* 12-*Val-de-Marne* 8, *rue du Général Sarrail*, 94 010 *Créteil Cedex*, *France*

(*Received on* 30 *May* 2001, *Accepted in revised form on* 19 *April* 2002)

This study describes the viscoelastic properties of a refined cellular-tensegrity model composed of six rigid bars connected to a continuous network of 24 viscoelastic pre-stretched cables (Voigt bodies) in order to analyse the role of the cytoskeleton spatial rearrangement on the viscoelastic response of living adherent cells. This structural contribution was determined from the relationships between the global viscoelastic properties of the tensegrity model, i.e., normalized viscosity modulus (η^*), normalized elasticity modulus (E^*), and the physical properties of the constitutive elements, i.e., their normalized length (L^*) and normalized initial internal tension (T^*). We used a numerical method to simulate the deformation of the structure in response to different types of loading, while varying by several orders of magnitude L^* and T^*. The numerical results obtained reveal that η^* remains almost independent of changes in T^* ($\eta^* \propto T^{*+0.1}$), whereas E^* increases with approximately the square root of the internal tension T^* (from $E^* \propto T^{*+0.3}$ to $E^* \propto T^{*+0.7}$). Moreover, structural viscosity η^* and elasticity E^* are both inversely proportional to the square of the size of the structure ($\eta^* \propto L^{*-2}$ and $E^* \propto L^{*-2}$). These structural properties appear consistent with cytoskeleton (CSK) mechanical properties measured experimentally by various methods which are specific to the CSK micromanipulation in living adherent cells. Present results suggest, for the first time, that the effect of structural rearrangement of CSK elements on global CSK behavior is characterized by a faster cellular mechanical response relatively to the CSK element response, which thus contributes to the solidification process observed in adherent cells. In extending to the viscoelastic properties the analysis of the mechanical response of the cellular 30-element tensegrity model, the present study contributes to the understanding of recent results on the cellular-dynamic response and allows to reunify the scattered data reported for the viscoelastic properties of living adherent cells.

*Corresponding author. INSERM UMR 492 Fonctions Cellulaires et Moléculaires de l'Appareil Respiratoire et des Vaisseaux, Faculté de Médecine, 8, rue du Général Sarrail, 94 010 Créteil Cedex, France. Tel.: +33-1-49-81-36-93; fax: +33-1-48-98-17-77.

E-mail address: patrick.canadas@creteil.inserm.fr (P. Cañadas).

Introduction

Cellular response to surrounding mechanical stresses as well as cellular deformation are critical for living cell functions such as differentiation, growth, wound healing, protein synthesis

0022-5193/02/$35.00/0

and proliferation (Bereiter-Hahn & Lüers, 1994; Elson, 1988; Planus *et al.*, 1998). Both geometry and mechanical responses of living adherent cells are now known to be mainly determined by the cytoskeleton (CSK), a three-dimensional pre-stretched structure of interconnected filamentous biopolymers (microtubules, microfilaments or actin filaments and intermediate filaments) which ensures high deformability and stabilization of the cell structure (Dennerll *et al.*, 1988; Heidemann & Buxbaum, 1990; Heidemann *et al.*, 1999). Indeed, the reported data exhibit a cellular response, often characterized by a non-linear mechanical behavior (e.g. the stress-hardening response of the CSK) and by a pre-stress dependence of cellular stiffness. Such a behavior has been attributed to the structural properties of the CSK considering that the overall mechanical properties of the CSK are strongly related to the spatial rearrangement of the CSK-filaments (Ingber & Folkman, 1989; Ingber, 1997, 1998; Ingber & Jamieson, 1985; Ingber & Karp, 1991; Wang & Ingber, 1994) and thus can be advantageously explained by the tensegrity concept (Ingber, 1993, 1998; Ingber *et al.*, 1994, 1995; Wang & Ingber, 1994; Wendling *et al.*, 1999, 2000a, b). Theoretical descriptions of tensegrity structure at the cellular level have been initially given by Stamenovic's group (Coughlin & Stamenovic, 1997, 1998; Stamenovic *et al.*, 1996), whereas other theoretical studies have provided normalized predictions of the mechanical behavior which all confirmed the expected nonlinear and pre-stress-dependent behaviors (Wendling *et al.*, 1999, 2000a). Noteworthy, the tensegrity models proposed up to now to describe the CSK response have only been studied in terms of pure elastic behavior, i.e. ignoring the structural viscous dissipation (Stamenovic & Coughlin, 1999, 2000; Stamenovic & Wang, 2000; Volokh *et al.*, 2000; Wendling *et al.*, 1999, 2000a, b). However, viscoelastic behavior could not be ignored when measuring the cellular or tissue response, as shown by many authors (Butler *et al.*, 1991; Evans & Yeung, 1989; Fredberg & Stamenovic, 1989; Fung, 1981; Heidemann *et al.*, 1999; Hochmuth & Waugh, 1987; Laurent *et al.*, 2002; Mathur *et al.*, 2000; Nemoto, 1982; Ragsdale *et al.*, 1997; Satcher & Dewey, 1996; Sato *et al.*, 1990; Thoumine & Ott, 1997; Valberg & Albertini, 1985; Wang & Ingber, 1994; Yamada *et al.*, 2000). Recently, using oscillatory magnetic twisting cytometry, Maksym *et al.* (2000) have shown that the elastic energy stored in human airway smooth muscle cells is coupled, via the cytoskeleton structure, to viscous-related frictional energy losses associated with viscous mechanisms. Thus, there is a great need to determine the contribution of spatial reorganization of CSK-filaments to the overall viscoelastic response of stretched cells.

Very few of the various theoretical models proposed to analyse the mechanical properties of adherent living cells, simultaneously consider: (i) the discrete nature of the cytoskeleton, (ii) the cell–cell and/or cell–extracellular matrix (ECM) interactions, and (iii) the cellular pre-stress. Advantageously, the 30-element tensegrity structure satisfies criteria (i)–(iii) above (Stamenovic & Coughlin, 2000; Stamenovic & Wang, 2000; Volokh *et al.*, 2000; Wendling *et al.*, 1999, 2000a, b). It thus appeared to constitute, at the onset of this study, a reasonable compromise to represent the complex interrelations between the structural polymeric organization and the mechanical behavior of the CSK. To predict the specific roles of internal tension and spatial rearrangement of the CSK-filaments on the viscoelastic response of the overall CSK structure, we then modified the classical 30-element tensegrity model in order to consider the viscoelastic properties of cables instead of non-viscous elastic properties exclusively considered in previous studies (Wendling *et al.*, 1999, 2000a,b). The viscoelastic response of the overall tensegrity structure was numerically studied by computing the structural response to creep tests over a large range of ''initial'' states of overall deformation (ε_i), i.e. from $\varepsilon_i = 0\%$ (corresponding to the reference state of the tensegrity structure when no external force is applied) up to $\varepsilon_i = 60\%$ (corresponding to a deformed state, where the tensegrity structure is highly stretched). This relatively wide range of ε_i-values actually corresponds to a wide variety of spatial organizations for the structure, i.e. from a symmetrical spatial organization of elements associated with a uniform distribution of local stress throughout elements ($\varepsilon_i = 0\%$) to an

increasingly asymmetrical organization associated with a more and more anisotropic distribution of local stresses as ε_i increases up to 60%. This range of initial deformation values aims at mimicking the wide variety of stretched states of the CSK-structure, including uniform and non-uniform distributions of stress throughout CSK-elements, as it can be encountered in living adherent cells (Ingber, 1993; Ingber *et al.*, 2000; Ingber & Jamieson, 1985). In addition, comparison between present theoretical results with experimental results was conducted for a variety of typical mechanical loading, i.e. extension, compression, shear and torque, moreover, exerted according to specific axis of the basal 30-element tensegrity structure, i.e. perpendicular or in parallel to the direction of bars. To approach the complexity of physiological loading conditions, we presently consider that forces externally applied (and associated displacements) may be seen as a combination of elementary loadings (i.e. extension, compression, shear and torsion) (Bruhat, 1955), and corresponding elementary displacements (i.e. translation, rotation), hence the idea of testing the structure with different types of elementary loadings, calculating first-order displacements in the direction of the load and neglecting the second-order displacements not directed in the direction of the load, as assumed in previous tensegrity studies (Coughlin & Stamenovic, 1997, 1998; Stamenovic & Coughlin, 1999, 2000; Stamenovic *et al.*, 1996; Wendling *et al.*, 1999, 2000a, b). In terms of biological responses, the different types of external loading applied to the cell contribute to a variety of spatial rearrangements of the structural CSK-elements that might constitute as much as specific mechanotransduction pathways, all necessary for the control of cellular functions (Ingber, 1993).

Comparison between structural behavior and cellular properties was performed, as in previous studies (Wendling *et al.*, 1999, 2000a, b), by assimilating the structure to an equivalent viscoelastic continuum embedding the structure whose mechanical properties provide the best fit of the numerical data. The mechanical properties of the overall tensegrity structure were therefore analysed, like cells, by calculating a unique couple of values, respectively, for viscosity and elasticity moduli, with the difference that the ratio of the axial to shear elastic modulus of the structure does not have to obey a continuous medium. To cover the most likely huge range of characteristic values taken by the physical properties of CSK-elements, the structural viscoelastic properties of the tensegrity model were normalized by the physical properties of constitutive elements. Experimental data used for comparison with numerical data pertaining to the tensegrity model were obtained by reanalysing previously published data obtained in living adherent epithelial cells in which the CSK is mechanically stretched by beads which are specifically attached to transmembrane receptors linked to the actin cytoskeleton.

Method

CHARACTERISTICS OF THE THEORETICAL TENSEGRITY MODEL

The 30-element tensegrity structure shown in Fig. 1 has already been studied under steady-state conditions (Stamenovic *et al.*, 1996) and more particularly to determine the relationships between the overall stiffness of the structure and the physical parameters of the constitutive elements (Wendling *et al.*, 1999). This tensegrity structure is composed of six rigid bars compressed by a continuous network of 24 pre-stretched cables.

To study the viscoelastic behavior of this 30-element tensegrity model, the cables were assumed to behave like viscoelastic Voigt bodies (elastic element in parallel with viscous dashpot). The Young modulus (E_p) and cross-sectional area (S_p), given to characterize the two types of elements (cables and bars), were taken to be constant (subscript "p" refers to the element (cables or bars), "c" to the cable and "b" to the bar). The values of viscosity modulus (η_c) of the cables and the length (l_b) of the bars are allowed to vary by several orders of magnitude.

In the reference state, i.e. when no external force is applied, the bars are aligned in pairs in the direction of coordinate axes (Fig. 1). This stable and symmetrical shape of the structure corresponds to the equilibrium between tension

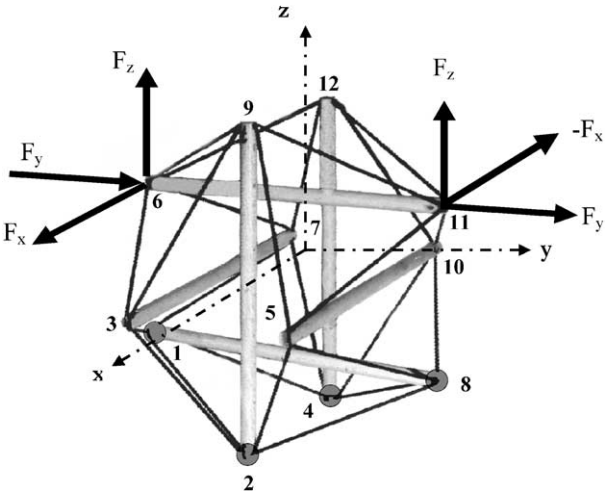

FIG. 1. Spatial view of the tensegrity structure studied (six bars and 24 viscoelastic cables). At the reference state (no external forces applied to the structure), the four nodes {#1, #2, #4, #8} are anchored and fixed in their spatial positions (●). The rectangular base $\{x, y, z\}$ is the referential system. External forces are applied at nodal points {#6, #11}. Extension and compression forces (F_z) are applied along the z-axis. Shear forces (F_y) are applied along the y-axis and the structure is submitted to a twisting torque by opposite forces applied at node #6 (F_x) and at node #11 ($-F_x$). We only consider first-order displacement in the direction of applied force. Second-order displacements, occurring at large deformation especially in shear, are not considered. The overall deformation resulting from application of external forces, is calculated by reference to the length L_0, defined as the distance between the inferior and the superior planes of the structure at reference state. To calculate the overall structural stress, we used a reference circular area S_0 (diameter L_0) embedding the structure.

($T_c^{(r)}$) in the cables and compression ($T_b^{(r)}$) in the bars, leading to the following relationships (exponent "r" corresponds to the reference state) (Mohri & Motro, 1993; Pugh, 1976):

$$\frac{l_c^{(r)}}{l_b} = \frac{\sqrt{6}}{4}, \tag{1}$$

$$\frac{T_c^{(r)}}{T_b^{(r)}} = \frac{\sqrt{6}}{6}. \tag{2}$$

NODAL ATTACHMENT AND LOADING CONDITIONS OF THE TENSEGRITY MODEL

The viscoelastic tensegrity model was subjected to uniaxial extension or compression so that the parallel bars [1–8] and [6–11] were either pulled apart or brought closer together by external forces applied at the endpoints (nodes {#6, #11}). During shear, the forces were applied at the nodes {#6, #11} along the corresponding rigid bar axis and during torque, the forces applied at these two nodes were opposite and perpendicular to the bars [6–11] and [4–12] (see Fig. 1). The bottom nodes {#1, #2, #4 and #8} remained fixed during deformation of the tensegrity structure in order to mimic cellular attachment to a non-deformable and non-planar substratum.

CONSTITUTIVE EQUATIONS OF THE THEORETICAL MODEL

The constitutive equations describing the dynamic behavior of the viscoelastic tensegrity model are derived based on the equations described previously in the case of pure elastic tensegrity model (Wendling *et al.*, 1999) applied, in the present study, to the viscoelastic behavior of cables. Taking into account the time dependence of cable properties and assuming small displacements, the methodology consists in resolving the following system of differential equations:

$$\{F\} = [K] \cdot \{u\} + [C] \cdot \{\dot{u}\}, \tag{3}$$

where the external-forces vector $\{F\}$ is related to both (i) the nodal-displacement vector $\{u\}$ associated with the global-rigidity matrix $[K]$, and (ii) the rate of nodal-displacement vector $\{\dot{u}\}$ associated with the global-damping matrix $[C]$. $\{F\}$ is a 1×36-column vector composed of the three-dimensional components of external forces applied at the 12 nodes. Similarly, the vector size of both nodal displacements $\{u\}$ and rate of nodal displacement $\{\dot{u}\}$ is a 1×36-column. The overall rigidity matrix $[K]$ is a Boolean sum of each elementary rigidity matrix $[K]_p$ [see eqn (4) and Wendling *et al.*, 1999] which depends exclusively on the Young modulus E_p, the internal force T_p (i.e., tension in the cables or compression in the bars), the cross-sectional area S_p and the length l_p of the element "p" as

follows:

$$[K]_p = \begin{bmatrix} \frac{E_p \cdot S_p - T_p}{l_p} c_x^2 + \frac{T_p}{l_p}; & \cdot & \text{symmetric} \\ \frac{E_p \cdot S_p - T_p}{l_p} c_x \cdot c_y & \frac{E_p \cdot S_p - T_p}{l_p} c_y^2 + \frac{T_p}{l_p}; & \cdot \\ \frac{E_p \cdot S_p - T_p}{l_p} c_x \cdot c_z & \frac{E_p \cdot S_p - T_p}{l_p} c_y \cdot c_z & \frac{E_p \cdot S_p - T_p}{l_p} c_z^2 + \frac{T_p}{l_p} \end{bmatrix}, \quad (4)$$

where the position of the element (p) resulting from spatial reorganization of the structure is taken into account by the elementary director cosines (c_x, c_y and c_z).

Similarly, the global-damping matrix $[C]$ is a Boolean sum of the elementary-damping matrix $[C]_c$ of each cable that depends on the viscosity (η_c), cross-sectional area (S_c) and length (l_c) of a given viscoelastic cable:

$$[C]_c = \begin{bmatrix} \frac{\eta_c \cdot S_c}{l_c} c_x^2; & \cdot & \text{symmetric} \\ \frac{\eta_c \cdot S_c}{l_c} c_x \cdot c_y & \frac{\eta_c \cdot S_c}{l_c} c_y^2; & \cdot \\ \frac{\eta_c \cdot S_c}{l_c} c_x \cdot c_z & \frac{\eta_c \cdot S_c}{l_c} c_y \cdot c_z & \frac{\eta_c \cdot S_c}{l_c} c_z^2 \end{bmatrix}. \quad (5)$$

As already mentioned by previous authors (Argyris & Scharpf, 1972; Wendling *et al.*, 1999), the rigidity matrix eqn (4) may be written as the sum of (i) an "elastic"-rigidity matrix (i.e., $(E_p S_p)/l_p$ terms) and (ii) a "geometric"-rigidity matrix (i.e., (T_p/l_p) terms), by contrast to the damping-viscosity matrix eqn (5) due to the independence of the viscous dissipation in cables on the level of initial strain (and also internal tension) in our model i.e., eqns (3) and (5). Through the cosine dependence of matrix terms appearing in eqns (4) and (5), the global rigidity $[K]$ and the damping $[C]$ matrices both reflect the spatial organization and the viscoelastic properties of the structural elements. Accordingly, the terms of $[K]$ and $[C]$ matrices values are specific to each level of structural deformation (i.e., ε_i defined as indicated below), which was present in the range $\varepsilon_i = 0\%$ (i.e., reference state with no external force applied)–60% (i.e., large deformation state). Therefore, equilibrium equation system eqn (3) was solved for small variations of force and displacement hypothesis (i.e., $\varepsilon \leqslant 0.05\%$), considering a linear Euler incremental method similar to the one used in previous studies. Note that the large deformation of the structure at initial state (i.e., ε_i values up to 60%) resulted from the summation of these elementary incremental deformations (i.e., $\varepsilon < 0.05\%$) (Argyris & Scharpf, 1972; Crisfield, 1991; Wendling *et al.*, 1999, 2000a). Once linearized, eqn (3) becomes eqn (3′):

$$\{\mathrm{d}F_i\} = [K(U_{i-1})] \cdot \{\mathrm{d}U_i(t)\} + [C(U_{i-1})] \cdot \{\mathrm{d}\dot{U}_i(t)\} \quad (3')$$

in which matrix coefficients $[K(U_{i-1})]$ and $[C(U_{i-1})]$, taken to be constant in this small range of $\{\mathrm{d}F_i\}$ and $\{\mathrm{d}U_i(t)\}$ variations, were determined from the preceding equilibrium state (subscript "$i-1$"), actually representative of initial deformation, i.e., before performing the undergoing creep test (subscript "i"). Then, the exact analytical solution of eqn (3) [or eqn (3′)] is given for each "actual" increment "i" by [Arnold, 1973; Coppel, 1965; Gantmacher, 1966; see also Fung, 1981, scalar eqn (11), p. 43]:

$$\{\mathrm{d}u_i\} = [I_d - \exp(-[C_{i-1}]^{-1}[K_{i-1}] \cdot \mathrm{d}t)] \cdot [K_{i-1}]^{-1}\{\mathrm{d}F_i\}, \quad (6)$$

which assumes zero nodal displacement at time $t = 0$ and where I_d represents the identity matrix (dimension: $[36 \times 36]$). The exponential-matrix operator (dimension $[36 \times 36]$) is defined as the convergence of the Taylor series of the corresponding matrix. Numerical points of creep tests were obtained by solving eqn (6) for several

incremental times (dt), i.e. by calculating several nodal displacements vs. time and verifying that creep nodal displacements systematically converged toward the non-viscous elastic solution. Time constant (τ) and apparent elasticity modulus (E) of the overall tensegrity structure were obtained by ($\varepsilon - t$)-curve-fitting analysis (KaleidaGraph™ software) over a large range (i.e., $\varepsilon_i = 0-60\%$) of initial states of overall deformation (Fig. 2). The curve-fitting analysis was performed assuming an equivalent continuous medium embedding the entire structure, i.e., a cylinder of height and cross-sectional diameter l_b. The apparent initial deformation ($\varepsilon_i = \Delta l / l_b$) of the overall tensegrity structure was calculated from the nodal displacement along the loading axis (Δl) divided by the length of a bar (l_b). This equivalent continuous medium was assumed to behave as a Voigt model submitted to a force equivalent to that applied to the structure and had a single elastic element in parallel with a unique viscous frictional element (and thus a single time constant) in the direction of the applied force. Amongst the various curve fitting tested such as logarithmic functions and a sum of exponentials functions with different time constants, the simple Voigt model provided the most satisfactory curve fitting of the numerical data as shown in Fig. 2 ($R^2 > 0.98$). This Voigt model was found to characterize the viscoelastic behavior of the tensegrity structure during the creep tests presently performed (i.e. the forces are not cyclically applied but remain constant after a step function of loading). In a recent study, Fabry *et al.* (2001) have shown that both elasticity (storage) and viscosity (loss) moduli follow a power law of the forced frequency. In the present creep tests, however, the power law did not appear to be an appropriate curve-fitting mathematical model to characterize the viscoelastic behavior of the studied tensegrity structure, likely because, by contrast to mechanical experiments in cells, elementary function of constant loading was used. In addition, when the vectors and matrices of eqn (6) are reduced to scalars the actual eqn (6) corresponds exactly to the creep function of a simple Voigt element.

We analysed the structural response in terms of viscosity modulus (η) deduced from the values of time constant (τ) and apparent elasticity

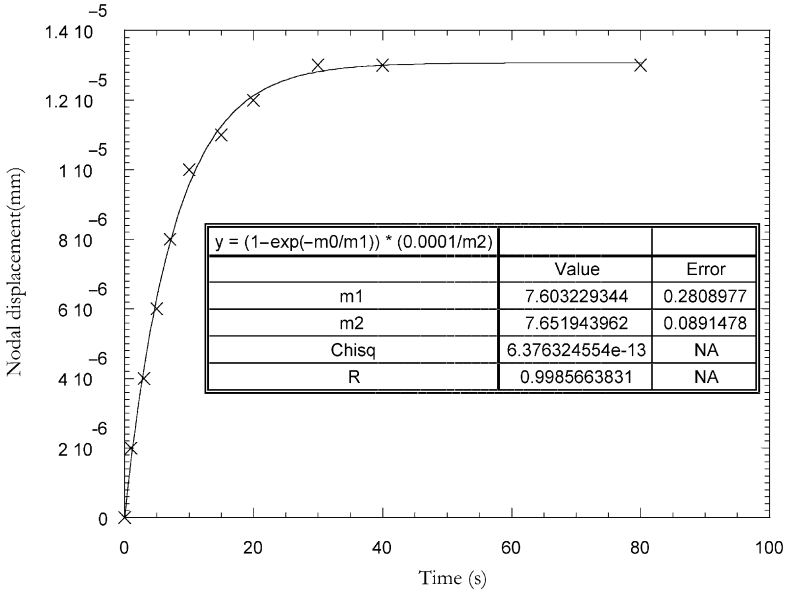

FIG. 2. Typical data obtained by simulation of creep tests performed with the 30-element tensegrity structure. The numerical points (×) correspond to the time variation of the displacement in the direction of the force of nodal points which are also the points of application of the forces. The curve fit was obtained assuming an equivalent continuous viscoelastic "solid" (see section Methods) with a constant rigidity ($m2$) and a unique time constant ($m1$). Other curve fits were tested, such as logarithmic functions and various sums of exponentials with different time constants, but none of them provided a fit of the numerical data as good as present viscoelastic "solid" (lower correlation coefficient R were obtained for the latter curve fittings).

modulus (E):

$$\eta = \tau \times E. \tag{7}$$

Viscosity modulus as a function of initial global deformation was then analysed for various initial states of deformation of the overall tensegrity structure submitted to various types of loading (extension, compression, shear and torsion).

NON-DIMENSIONAL ANALYSIS

In order to analyze the time constant (τ) and viscosity modulus (η) of living cells at a microscopic scale and to determine the scale effect and dependence of the cellular mechanical response on the specific properties of the constitutive polymeric filaments, non-dimensional quantities were defined by

$$T^* = \frac{T_c^{(r)}}{(ES)_c}, \tag{8}$$

$$L^* = \frac{l_b}{r_b}. \tag{9}$$

The normalized elastic tension T^*, which corresponds to the elastic strain of the cables (below, the term overall "deformation" pertains to the entire tensegrity structure while the term local "strain" pertains to its constitutive elements) at the reference state, quantifies the basal level of internal tension in the tensegrity structure. The normalized length L^* defines the characteristic scale of the overall 30-element tensegrity structure: the smaller L^*, the smaller the size of the structure, and thus, the smaller the free-space volume in between the constitutive elements (r_b is the bar radius). Apparent elasticity modulus (E), time constant (τ) and viscosity modulus (η) of the viscoelastic tensegrity model were all normalized using the mechanical properties of a given viscoelastic cable, thus allowing an expression of the overall properties proportional to the properties of individual elements:

$$\tau^* = \frac{\tau}{\tau_c}, \tag{10}$$

$$E^* = \frac{E}{E_c}, \tag{11}$$

$$\eta^* = \frac{\eta}{\eta_c}. \tag{12}$$

The normalized overall properties of the tensegrity structure were studied in terms of normalized length L^* and normalized elastic tension T^* of its constitutive elements [eqns (7)–(12)].

Results

Normalized viscoelastic properties of the overall tensegrity structure, i.e., apparent elasticity modulus E^*, time constant τ^* and viscosity modulus η^*, resulting from numerical resolution of constitutive equations of the model [eqns (8)–(9)], are presented in Figs 3–7 as a function of the initial value of global deformation ε_i as well as the normalized properties of the constitutive elements, i.e., length L^* and internal tension T^* at reference state. The use of non-dimensional forms to describe the viscoelastic properties of the tensegrity model illustrates a fundamental property of tensegrity structures, i.e., the viscoelastic properties of the overall tensegrity

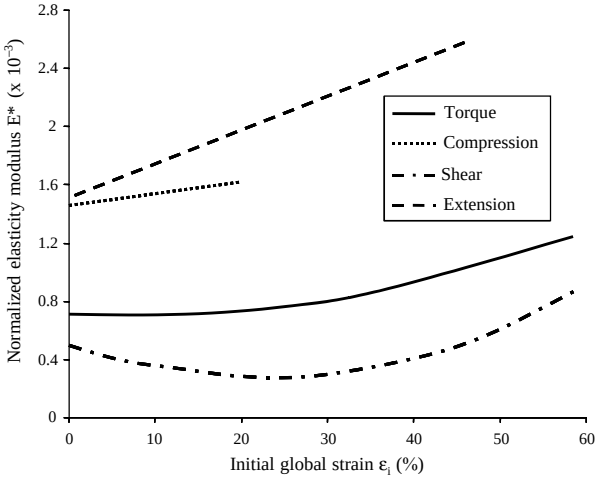

FIG. 3. Normalized elasticity modulus of the overall tensegrity structure as a function of the global deformation ε_i obtained by numerical simulations of creep tests performed for the four types of tested loading, i.e. extension, compression, shear and torque. The low value of maximal deformation tested in compression ($\varepsilon_i \approx 20\%$) is due to the fact that bars [6–11] and [3–7] or [5–10] get into contact at this level of overall deformation (see also Fig. 1).

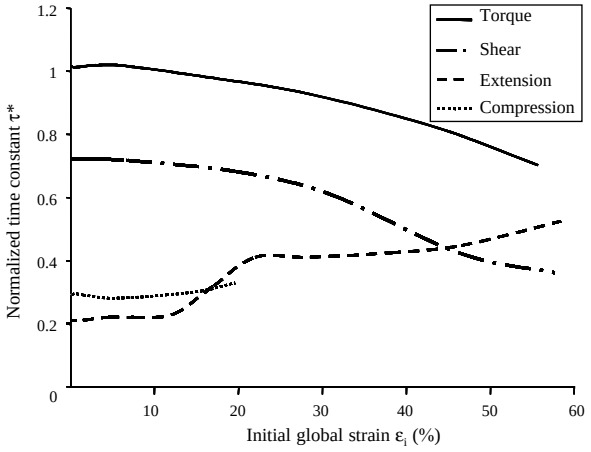

FIG. 4. Normalized time constant τ^* of the overall tensegrity structure as a function of the global deformation ε_i obtained by numerical simulations of creep tests performed for the four types of applied loading (extension, compression, shear and torque). The creep curves obtained were fitted with KaleidaGraph™ software which provides the values of both E^* and τ^* with satisfactory correlation coefficients ($R > 0.98$).

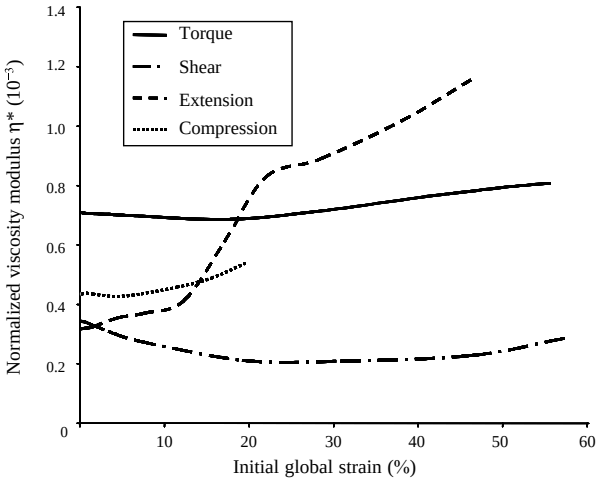

FIG. 5. Normalized viscosity modulus η^* of the overall tensegrity structure, as a function of the global deformation ε_i, calculated from the product of the corresponding normalized elasticity modulus E^* by normalized time constant τ^* [see eqn (7) for the four types of applied loading extension, compression, shear and torque].

structure are proportional to the viscoelastic properties of their constitutive elements. The reported dependencies of the viscoelastic properties of the model are expressed in terms of power-law of constitutive element properties in

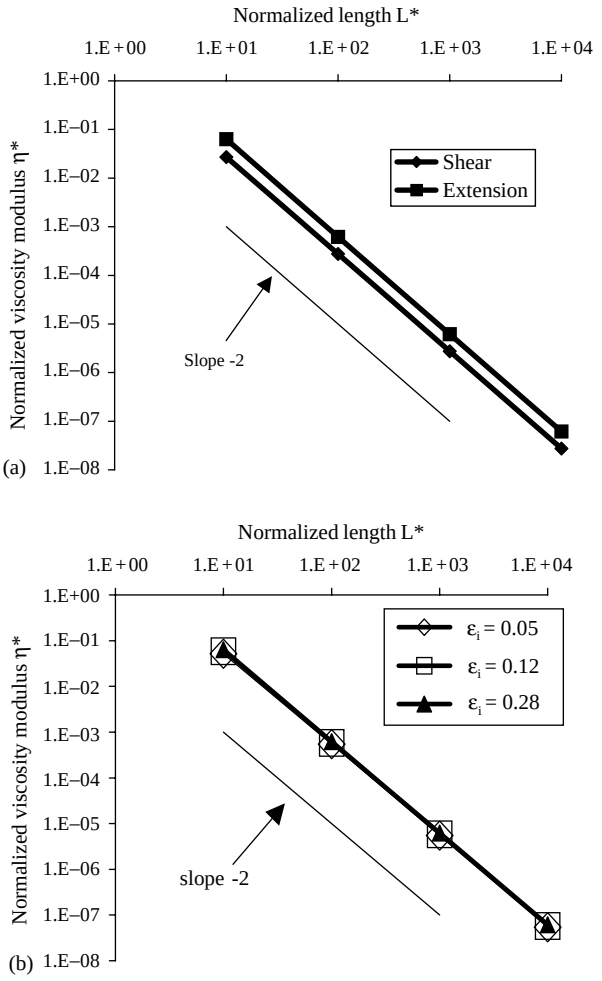

FIG. 6. Normalized viscosity modulus η^* of the overall tensegrity structure as a function of the normalized element length (corresponding to the size of the structure) L^*, (i) at given values of initial global deformation ($\varepsilon_i \approx 30\%$) and initial internal tension ($T^* = 0.25$) for shear and extension in (a); (ii) for extension force applied and three different values of global deformation ($\varepsilon_i \approx 5\%$, 15% and 30%). Note that the curves show a systematic negative logarithmic slope (−2) regardless of the type of loading applied and the values of global deformation ε_i. The values of overall viscosity modulus are always greater (by a factor of 4–5) in extension than in shear regardless of the value of L^*.

Table 1. Note that the present elasticity results were obtained under attachment and loading conditions which partly differed from those previously studied by Wendling *et al.* (1999), namely stretching in the direction of the bars with four fixed bottom nodes in the present study, instead of stretching at an angle of 45° from the initial direction of the bars with three attached nodes in previous study (Wendling *et al.*, 1999).

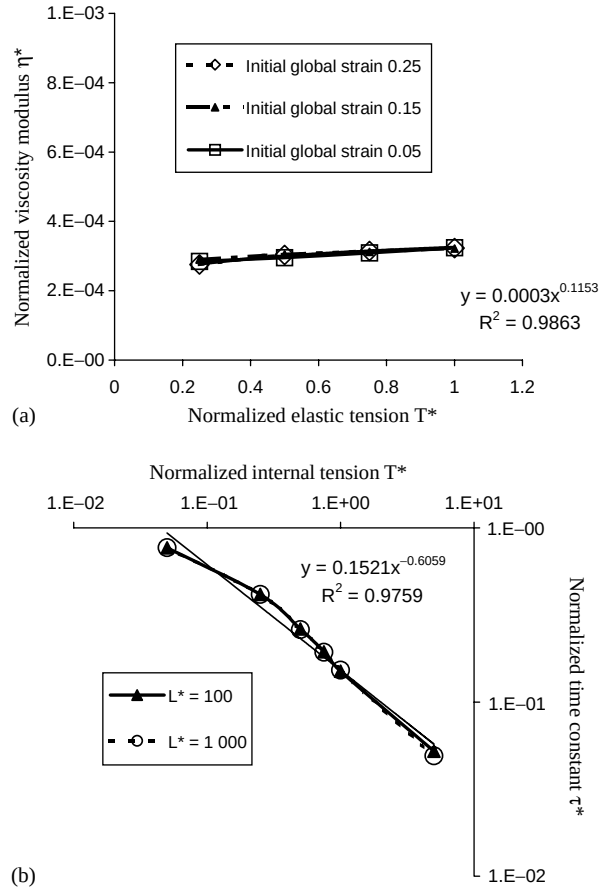

FIG. 7. Normalized viscosity modulus η^* (a) and time constant τ^* (b) of the overall tensegrity model as a function of the initial internal tension T^*. Viscosity modulus η^* is shown to increase non-significantly (logarithmic slope $\approx +0.1$) with increasing T^* and at given value of L^* ($L^* = 100$) regardless of the level of initial global deformation of the structure (a). The corresponding time constant τ^* decreases as the internal tension T^* increases, with a significantly negative logarithmic slope (-0.6) and at a given value of global structure deformation ($\varepsilon_i \approx 30\%$) regardless of the normalized element length L^* (b).

DEFORMATION DEPENDENCE OF THE VISCOELASTIC RESPONSE

The variations of the normalized apparent elasticity modulus E^* of the overall tensegrity structure for the four types of tested loading were analysed vs. initial deformation ε_i of the structure and for a given couple of L^* and T^* values, i.e., $L^* = 100$ and $T^* = 0.25$ (see Fig. 3). Extension and compression curves (upper curves) show that E^* remains proportional to initial deformation ε_i, while shear and torque curves (lower curves) exhibit a nonlinear increase of E^* with ε_i. Values of normalized elasticity modulus (E^*) appear therefore always higher in extension than in shear, with a ratio close to three at very low deformation values ($\approx 0.05\%$). This result suggests that the mechanical behavior of the tensegrity structure, in this small range of deformation, roughly mimics a continuous medium, i.e., the Poisson's ratio (ν) approaches a typical value of 0.5 while remaining slightly above (see the Appendix and Table 2). Incidentally, at higher values of ε_i, the Poisson's ratio of the tensegrity model (ν) is not constant and always greater than the standard Poisson's ratio of a continuous medium, i.e., $\nu > 0.5$ (see Table 2 and the Appendix). Present results obtained in specific attachment conditions are qualitatively similar to those previously obtained by Wendling *et al.* (1999), except for compression, for which the structure compressed in the direction of bars undergoes a stiffening process instead of a softening process obtained in previous study. Nevertheless, the one-order-of-magnitude difference in elasticity moduli observed between

TABLE 1

	Extension		Shear		L^*		T^*	
	$\varepsilon_i = 5\%$	$\varepsilon_i = 50\%$	$\varepsilon_i = 5\%$	$\varepsilon_i = 50\%$	Extension	Shear	Extension	Shear
E^*	0.0016 Fig. 3	0.0026 Fig. 3	0.0004 Fig. 3	0.0006 Fig. 3	$\propto L^{*-2}$ not shown	$\propto L^{*-2}$ not shown	$\propto T^{*0.3}$ not shown	$\propto T^{*0.7}$ not shown
τ^*	0.22 Fig. 4	0.47 Fig. 4	0.72 Fig. 4	0.40 Fig. 4	$\propto L^{*0}$ not shown	$\propto L^{*0}$ not shown	$\propto T^{*-0.2}$ not shown	$\propto T^{*-0.6}$ Fig. 7(b)
η^*	0.0003 Fig. 5	0.0012 Fig. 5	0.0003 Fig. 5	0.0002 Fig. 5	$\propto L^{*-2}$ Fig. 6	$\propto L^{*-2}$ Fig. 6	$\propto T^{*0.1}$ not shown	$\propto T^{*0.1}$ Fig. 7(a)

TABLE 2

Overall initial deformation ε_i (%)	Poisson's ratio
0	0.59
10	1.44
20	2.19
30	2.28
40	1.78

present study (i.e. $E^* \sim 10^{-3}$ in Fig. 3) and previous tensegrity study (i.e. $E^* \sim 10^{-4}$ in Wendling *et al.*, 1999) may be attributed to the differences in the specific stretching and attachment conditions.

The corresponding variations of the normalized time constant τ^* vs. initial deformation ε_i are presented in Fig. 4 for the four types of loading tested and $L^* = 100, T^* = 0.25$. The values of τ^* are quasi systematically less than 1, although never less than 0.2, i.e. $\tau \geqslant 20\%\tau_c$, indicating that spatial displacement of constitutive elements contributes to make shorter the time response of the overall structure regardless of the individual element response. For torsion and shear, the normalized time constant decreased continuously as ε_i increased (up to the studied limit of $\varepsilon_i = 60\%$), whereas for compression, time constant increased slightly from $\varepsilon_i =$ 0% to 20%. Note that, for compression, the structure cannot be deformed beyond 20% due to contact between horizontal bars [6–11] and [3–7] or [5–10]. For extension, the values of the time constant τ^* rapidly increased in an intermediate range of ε_i (= 13–22%) to reach, in the range ε_i (= 22–60%), values which are twice those obtained in the lower range of ε_i (= 0–13%). A transient loss of the pretension in the four upper cables between $\varepsilon_i \approx 13\%$ and 22% during extension explains the singular slope variations of the $(\tau^* - \varepsilon_i)$ curve observed in the 13–22% range of ε_i in Fig. 4.

The relationships between the normalized viscosity modulus η^* [see eqn (7)] and ε_i are presented in Fig. 5 for the four different types of loading tested and the same L^* and T^* values. The normalized viscosity modulus η^* varies slowly with ε_i except for extension where η^* increases with ε_i. In relation to the τ^*-increase with ε_i (Fig. 4), slope variations of the $(\tau^* - \varepsilon_i)$ curve are observed in the range $\varepsilon_i \approx 13-22\%$. Interestingly enough, values of η^* much lower than 1, illustrate a typical behavior of the model, i.e., the spatial rearrangement of constitutive elements largely contributes to the reduction of dissipated energy compared to individual elements.

LOCAL PROPERTIES DEPENDENCE OF THE GLOBAL VISCOELASTIC RESPONSE

The normalized viscosity modulus η^* of the tensegrity model was studied as a function of the local parameter $L^*(i)$ for fixed values of $\varepsilon_i (= 0.30)$, $T^* (= 0.25)$, and two types of loading: shear and extension [Fig. 6(a)], and (ii) for three levels of deformation ε_i (= 0.05, 0.12, 0.28), a fixed value of T^* (= 0.25) and extension loading [Fig. 6(b)]. The $(\eta^* - L^*)$ relationships, plotted on a double-logarithmic coordinates, exhibit a linear behavior with a slope of -2, indicating an exact L^{*-2}-dependence of η^*, both in shear and in extension [Fig. 6(a)] but with values of viscosity modulus in shear 4–5 times lower than those in extension (Fig. 5). This L^{*-2}-dependency seems to be not affected by the degree of initial deformation ε_i studied [Fig. 6(b)]. This L^{*-2}-dependence of η^* can be associated with the L^{*-2}-dependence of E^* observed in the present study as in previous tensegrity studies (Wendling *et al.*, 1999, 2000a, b) meaning that time constant of the tensegrity structure response is independent of the parameter L^* (not shown).

The normalized viscosity modulus η^* was also studied in shear as a function of the elastic cable strain T^*, for a fixed value of normalized bar length L^* (= 100) and for three different values of initial structural deformation ε_i (= 0.05, 0.15, 0.25) [Fig. 7(a)]. The $(\eta^* - T^*)$ relationships plotted on semi-logarithmic coordinates seem to be not dependent on the initial structural deformation ε_i and exhibit almost zero slope which expresses a negligible effect of T^* on η^* [Fig. 7(a)]. Still in shear, the time constant of the overall structure, τ^*, was plotted on double-logarithmic graph vs. T^*, for two values of L^* (= 100 and 1000) and a given value of initial structural deformation ε_i (= 0.30). It appears that τ^* decreases with a slope of -0.6 as initial cable strain T^* increases [Fig. 7(b)]. The corresponding $E^* - T^*$ relationships found in the

present study qualitatively resemble the data reported in previous tensegrity studies by Wendling *et al.* (1999, 2000a), i.e., a slope close to 0.5 on double-logarithmic coordinates. Precise values of $E^* - T^*$ slope are given in Table 1 which reveals that the T^*-dependence of E^* roughly compensates that of τ^*, in agreement with Fig. 7a.

Table 1 summarizes the above results and can be used to predict the quantitative relationships between the viscoelastic properties (E^*, η^*, τ^*) of the overall tensegrity structure and the mechanical and geometric parameters (T^*, L^*) of the constitutive elements (cables and bars). The T^*-dependence of E^* varies over the range $\{0.3–0.7\}$ and the T^*-dependence of τ^* varies over the range $\{-0.2;-0.6\}$, indicating that η^* remains quasi independent on T^*.

Discussion

The present study constitutes a first attempt to establish normalized power laws (summarized in Table 1) governing the relationships between the global properties of a cellular viscoelastic tensegrity model (E^*, η^*, τ^*) and the local properties of its constitutive elements (i.e. T^*, the cable strain and L^*, the normalized element length, both defined at reference state). These power laws are indeed nonlinear and characterize, in the privileged direction of loading and for a wide range of (i) element properties and (ii) initial states of global deformation, the overall effect on time constant, viscosity and elasticity of the three-dimensional rearrangement of the structure. Because of the similarities in viscoelastic behavior observed between tensegrity models and living adherent cells, it can be concluded that the present approach may provide a first quantification of the structural basis of cellular viscoelasticity.

STRUCTURAL ORIGIN OF CELLULAR VISCOELASTICITY

Although cellular viscosity has been observed in many micromanipulation experiments in living cells (Butler *et al.*, 1991; Evans & Yeung, 1989; Fredberg & Stamenovic, 1989; Fung, 1981; Heidemann *et al.*, 1999; Hochmuth & Waugh, 1987; Laurent *et al.*, 2002; Mathur *et al.*, 2000; Nemoto, 1982; Ragsdale *et al.*, 1997; Satcher & Dewey, 1996; Sato *et al.*, 1990; Thoumine & Ott, 1997; Valberg & Albertini, 1985; Wang & Ingber, 1994; Yamada *et al.*, 2000), the exact nature of the viscous dissipation process is not well understood. Some authors consider that viscous mechanisms are associated with shear stress in the cytoplasmic fluid (Fung, 1981; Fung & Liu, 1993; Heidemann *et al.*, 1999). Some others consider that cellular friction and cellular elasticity are both supported by the actin-filament network within the CSK (Satcher & Dewey, 1996). Accordingly, recent dynamic measurements on human airway smooth muscle cells suggest that frictional stresses, which cause mechanical energy dissipation through the cell, do not arise from cytoplasmic fluid flow, but rather are coupled to the elastic stresses associated with cytoskeleton distortion (Maksym *et al.*, 2000). On the whole, the physical origin of cellular friction remains an open question and none of the previous studies have provided clear explanations of how the CSK-structure dissipates energy in the course of spatial filament reorganization. Another related question is to whether pre-stress influences the cell viscoelastic response as already shown for the purely elastic response (Wendling *et al.*, 1999, 2000a, b). Although the present study does not pretend to examine the various mechanisms susceptible to dissipate energy within the cell cytoplasm, it permits a first quantification of the contribution of spatial redistribution of CSK-elements on cellular viscosity.

Present results suggest that the effect of spatial redistribution of CSK-elements on the viscoelastic cellular response can be predicted on the basis of the spatial viscoelastic tensegrity model. Based on the results obtained and in agreement with a volumetric fraction of constitutive elements which, in any case, remains much smaller than the volume occupied by the tensegrity structure, the global cellular mechanical properties are expected to be systematically smaller than local properties of the elements (Wendling *et al.*, 1999, 2000a, b). Interestingly, previous experimental observations are consistent with this prediction, i.e. values of cellular viscosity (up to 10^3–10^4 Pa s, see Fig. 8) and cellular elasticity (up to 10^4–10^5 Pa, see Fig. 12 in

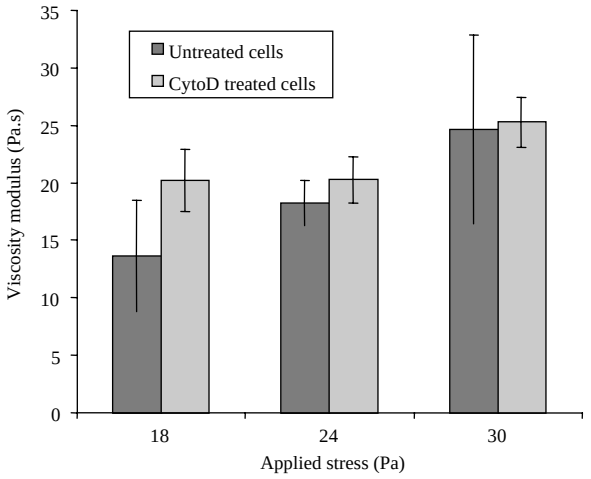

FIG. 8. Effect of actin filament depolymerization on CSK-viscosity of cultured A549 epithelial cells assessed by magnetic twisting cytometry. Viscosity values were established from the product of stiffness (stiffness data have already been published in Wendling *et al.*, 2000a) and relaxation time constant, for different levels of applied stress. Depolymerization of actin filaments was obtained by adding cytochalasin *D* to the culture of epithelial cells ($1\,\mu g\,ml^{-1}$) during 20 min. Note that, at any given stress, the CSK-viscosity was not significantly modified by the F-actin depolymerization. Each value is a mean $\pm$ SD over $n = 6$ wells. A549 epithelial cells were plated at a density of 30×10^3 cells well^{-1} and incubated for 24 hr. RGD-coated ferromagnetic beads were then added to the cells. The well was placed in the magnetic twisting cytometer. A brief 0.15 T magnetic pulse was applied to magnetize all surface-bound beads in a unique horizontal direction, and a magnetic torque was then generated by applying an orthogonal homogeneous magnetic field (<6.3 mT). Associated changes in angular strain of beads were measured by an on-line magnetometer. CSK-stiffness was defined by the ratio of applied stress to angular strain and viscosity was obtained by the product of time constant and stiffness.

Maksym *et al.*, 2000) are both several orders of magnitude smaller than reported values of F-actin viscosity (Janmey *et al.*, 1991; Janmey & Stossel, 1988) and elasticity (Kojima *et al.*, 1994).

Another important behavior that can be predicted from the spatially redistributed structure is the role of internal tension (pre-stress) on cellular mechanical properties. While tensegrity elasticity modulus was shown to increase with increasing internal tension, viscosity modulus remains almost constant when internal tension changes [see Table 1 and Fig, 7(a)]. Mathematically, the non significant T^*-dependence of $\eta^*(\propto T^{*+0.1})$ can be related to the absence of pre-stress-related geometric matrix in the damping "viscosity" matrix [see eqn (5)], while the overall rigidity matrix is a Boolean sum of elementary geometric matrix and elastic-rigidity matrix [see eqn (4) and Wendling *et al.*, 1999, 2000a)], hence the T^*-dependence of $E^*(\propto T^{*+0.5})$. However, the biological relevance of this result is unclear. In a previously published study, experimental measurements of rigidity modulus in cells were obtained using step twisting magnetic cytometry (Wendling *et al.*, 2000a). In this study, the alteration in pre-stress (internal tension) was modeled by treating cells with low concentrations of cytochalasin D, which tends to depolymerize actin filaments, resulting in a strong alteration in cellular elasticity modulus (Wendling *et al.*, 2000a). In the present study, we reanalysed these cellular data in order to extract the viscosity modulus and the time constant, thus extending earlier results. Values of cellular viscosity modulus obtained for three levels of applied stress are plotted in Fig. 8, for treated and untreated cells. As predicted by the tensegrity model, the decrease in CSK internal tension induced by microfilament depolymerization did not significantly affect the cellular viscosity modulus (see Fig. 8). Similar results were also found by Wang (1998) but the level of stress applied to the cells remained unchanged. Noteworthy, the use of various levels of applied stress (as in Fig. 8) not only extends Wang's results, but also allows to discuss the CSK-response in terms of thickening or solidifying process, as explained below. Note that, although we used a drug concentration ten times higher than that in Wang's study (i.e., $0.1\,\mu g\,ml^{-1}$ in Wang's study and $1\,\mu g\,ml^{-1}$ in present study), it has been suggested, based on microscopic observations, that disruption of actin filament network and particularly of stress fibers lattice was not obvious (Wendling *et al.*, 2000a). This means that cellular structural shape may not be significantly altered, while cellular internal tension would severely drop secondary to cytochalasin-D treatment (Wendling *et al.*, 2000a). By contrast, in another study, Wang & Ingber (1994) suggested that increasing cell spreading would produce a higher cellular tension which could increase cellular viscosity. However, present results obtained in extension reveal that structural viscosity tends to increase as initial strain increases (which can be seen as

mimicking an increase in cellular spreading), while increasing initial internal tension was not needed. In other words, the increase in cellular viscosity and cellular tone observed by Wang and Ingber could indeed be attributed to the increase in heterogeneity of the internal tension distribution throughout CSK-elements in more spreading cells, although other factors could also be mentioned such as the increase in the number and the strength of activated stress fibers in more spread cells (Wang & Ingber, 1994; see also present Fig. 5). In addition, very recent experimental findings obtained in smooth muscle cells with oscillated beads (Stamenovic *et al.*, 2002) have shown that the storage elastic modulus (G', corresponding to elastic stresses, proportional to the stored mechanical energy) and loss elastic modulus (G'', corresponding to frictional stresses, proportional to dissipated mechanical energy, viscosity being determined as the ratio of loss modulus to angular velocity: $\eta = G''/\omega$), both increased linearly with the level of cell contractile pre-stress (P) pharmacologically modified by providing graded doses of either relaxant agonist or contractile agonist. Strictly speaking, such a linear pre-stress (P)-dependence of loss modulus G'' (i.e. $G'' \propto P$) experimentally founded by Stamenovic *et al.* differs from the ($\eta^* \propto T^{*+0.1}$)-predictions given by the viscoelastic-tensegrity model presently studied, considering that P and T^* are by definition linearly related. These authors noticed, however, that the linear pre-stress dependence was found to be much smaller for the loss modulus than for the elastic modulus, which was expressed by a prefactor 4 times smaller for the loss modulus than for the elastic modulus. Note that the smaller pre-stress dependence of the loss vs. the storage elastic moduli which characterizes these experimental data qualitatively agrees with the mean prediction of our viscoelastic-tensegrity model (i.e. $T^{*+0.1}$ for η^* versus $T^{*+0.5}$ for E^*, see Table 1). A better insight of the tensegrity relevance can be obtained by fitting experimental data [i.e. those in Fig. 5(A) in Stamenovic *et al.*, 2002] using hyperbolic functions. Curve fitting with correlation coefficients $R^2 \geqslant 0.9$ could be obtained for $G'' = 5.64P^{+0.39}$ and $G' = 9.46P^{+0.5}$, which shows that experimental data remarkably agree with tensegrity-model predictions (see Table 1 for comparison) for the storage elastic modulus while the agreement is less obvious for the loss modulus results. Note that the pre-stress values used by Stamenovic *et al.* lie in a limited range of variation (one cycle) which justifies the linear regression assumption. A residual important difference between the Stamenovic *et al.* study and our theoretical study might reside in the definition of pre-stress. In the present study, as in our previous studies (Wendling *et al.*, 1999, 2000a), we defined the pre-stress by the normalized internal tension, T^*, a local parameter which corresponds to the initial extension of the constitutive cable of tensegrity structure, while in Stamenovic *et al.* (2002), the pre-stress, P, is global and corresponds to the total stress deduced from the resultant force (per unit area) exerted by all tensile elements on a gel substrate across a transsectional area of the cell (see also Wang *et al.*, 2002). More generally, the predictions obtained from the viscoelastic-tensegrity model should be modulated by the definition of the pre-stress and by the magnitude of pre-stress value considered. These differences, in addition to a number of mechanisms discussed by Stamenovic *et al.* (2002) (e.g., CSQ remodeling, nonlinear rheological properties of CSK-filament networks, friction arising between filaments, actomyosin kinetics), might also contribute to explain the measurable effects of pharmacologic drugs on loss modulus in the above smooth muscle cell experiments while depolymerization effects were not found significant in epithelial cells (Fig. 8).

As expected from the definition of the normalized time constant [eqns (7,10–12)], τ^* is independent on the structure size L^*, but depends on T^*: the higher T^*, the smaller τ^* (see results in Table 1). Because the time constant related to the viscoelastic-tensegrity model always remains smaller than the time constant of the viscoelastic elements whatever be the initial global deformation ε_i (i.e., $10^{-2} < \tau^* \leqslant 10^0$)—except in the case of torsion and at very small values of ε_i—it can be said that a more tensed tensegrity structure has a faster response than a less-tensed structure, which tends to weakens the viscous effects. This tensegrity-model behavior indeed characterizes the structural viscoelasticity of spatially

rearranged pre-stressed systems of very different sizes and element properties including those encountered at the microscale in living cells.

It should be stressed that both cellular viscosity (presented in Fig. 8) and cellular elasticity moduli [Fig. 6(a) in Wendling *et al.*, 2000a] appear to agree with the theoretical predictions given by the viscoelastic-tensegrity model. Moreover, the stress-dependence of cellular viscosity modulus shown in Fig. 8 suggests that the CSK-structure exhibits a stress-thickening behavior which can be predicted by viscoelastic-tensegrity model during extension (Fig. 5). This stress-thickening behavior exists in parallel to the largely reported stress-stiffening behavior [see also Fig. 6(a) in Wendling *et al.*, 2000a] and was not indicated in previous study (Wang, 1998). Incidentally, the decrease in time constant, observed with increasing the initial internal tension [Fig. 7(b)], reflects a tone-associated "solidifying" behavior of the tensegrity structure.

Recent results obtained by Maksym *et al.* (2000) also appear not to contradict the predictions given by the viscoelastic-tensegrity model. Indeed, addition of cytochalasin D to human airway smooth muscle cell culture resulted in a great decrease in the storage elastic modulus (G') while the loss frictional modulus (G'') was found to remain roughly constant (see Fig. 10 in Maksym *et al.*, 2000) in agreement with present results. Moreover, to describe the coupling between frictional energy loss and elastic energy storage, Fredberg and Stamenovic proposed to estimate the so-called hysteresivity $h(= G''/G')$, to better characterize the biological material (Fredberg & Stamenovic, 1989). Hysteresivity has been found to increase considerably in treated cells (Maksym *et al.*, 2000). An alternate definition of hysteresivity is $h = \tau \times \omega$, showing that dimensions of time constant τ and hysteresivity h only differ by "s^{-1}". Although in the present study, the forces are not exerted at a characteristic forced frequency (creep tests), the so-called hysteresivity can, in that case, be attained by dividing the global time constant by a second characteristics time, e.g., the local one. Consequently, the normalized time constant (τ^*), defined in eqn (10) plays, in the present transient conditions, a role equivalent to that of hysteresivity h in oscillatory conditions. It is remarkable that the "cytochalasin D"-dependence of G', G'' and h measured in living cells by Maksym *et al.* (2000) could advantageously be explained by the T^*-dependence of E^*, η^*, and τ^*, which characterizes the structural viscoelasticity, as predicted by the viscoelastic-tensegrity model presently studied.

In summary, the strong analogies between the cell-mechanical behavior and the tensegrity-structure behavior suggest that both elastic and dissipative properties measured in living cells are intrinsically related to the CSK-structure, thus confirming the assumptions of previous authors (Janmey *et al.*, 1991, 1989; Janmey & Stossel, 1988; Maksym *et al.*, 2000; Satcher & Dewey, 1996). It means that the viscoelastic properties of certain CSK-elements, e.g., the actin filaments, in conjunction with their spatial rearrangement might govern cellular viscoelastic properties, which does not exclude other possible dissipative mechanisms arising from the other components of the cytoplasm such as the nucleus (Caille *et al.*, 2001) or the membrane.

BIOLOGICAL RELEVANCE OF TENSEGRAL VISCOELASTICITY

Previous studies performed on tensegrity structures with purely elastic elements have revealed that living cells and tensegrity models share a number of common structural and mechanical features (Coughlin & Stamenovic, 1997; Stamenovic *et al.*, 1996; Volokh *et al.*, 2000; Wendling *et al.*, 1999). We are aware that studied tensegrity models are based on a number of simplifying assumptions compared to the complexity of the CSK-network, e.g., smaller number of elements, homogeneity of their properties, limited number of interconnections and simplified loading conditions compared to physiological conditions. However, it has been argued that simplified tensegrity structure could yet be representative of more complex tensegrity structures (Kebiche *et al.*, 1996; Mohri & Motro, 1993), while theoretical results confirm that main features, e.g., the L^*; T^*; ε_i-effects, of different tensegrity models even studied in a variety of attachment and loading conditions, do not

fundamentally diverge (Wendling *et al.*, 1999, 2000a, b). Concerning the simplified loading conditions, it can be said that every complex force applied by the environment on the cell could be decomposed as the sum of elementary forces such as those presently studied, and that such an analysis would anyway require a proper evaluation of elementary stresses such as the one presently done.

We focus in this study on the viscoelastic dissipation in a cellular-tensegrity model which is induced by the spatial rearrangement of viscoelastic elements. Structural pre-stress arises from a tension in viscoelastic elements which is counterbalanced by compression in rigid bars. It has been recently shown that various polymeric elements are able to support even opposed mechanical efforts (Ingber & Karp, 1991; Heidemann & Buxbaum, 1990; Ingber, 1993), basically tension in actin filaments and compression in microtubules. Initial studies on CSK biopolymer solutions have demonstrated the viscoelastic behavior of actin filaments which appear to be the major CSK-components responsible for cellular viscosity (Janmey *et al.*, 1991, 1989; Janmey & Stossel, 1988). Recent studies have shown that isolated stress fibers behave as truly contractile structures, even once separated from the contractile cell cortex (Katoh *et al.*, 1998). Indeed, in living cells, internal tension may be generated actively in the cell's actomyosin-based contractile apparatus or passively by distension of actin filament due to external forces applied through extracellular adhesions. On the other hand, microtubules, whose solutions also appear viscoelastic, would rather behave as rigid rod-like polymers when they are crosslinked with other CSK-filaments, e.g., intermediate filaments, which could constraint the buckling effect (Janmey *et al.*, 1991; Brodland & Gordon, 1990). Moreover, it is not obvious that forces transmitted at the cellular scale level are sufficient to permit microtubule buckling (Stamenovic & Coughlin, 1999). In a recent study using traction force microscopy, Wang *et al.* (2001) have firmly demonstrated that microtubules bear compression and are thus responsible for a significant portion of cellular pre-stress. More generally, the living cell is in constant interaction with its close microenvironment, and the system constituted by the "adherent cell structure" coupled to "a relatively non-flexible ECM" would then behave as a pre-stressed viscoelastic structure (Wendling *et al.*, 2000a). Thus, it is to notice that at different scale level, a variety of elements are also able to support local compression such as the integrin complex linked to the non-flexible ECM (Ingber, 1997; Ingber *et al.*, 1994). The tensegrity model precisely takes into account the interconnectedness between the two different types of CSK-substructures including tensed viscoelastic elements and compressed "rigid" elements. Considering that viscoelastic elements may represent actin assemblies, it has been shown that actin filament can be stretched up to 20% without disruption (Janmey *et al.*, 1991), whereas wider actin stress fibers, which are known to represent a prototype of striated muscle sarcomere, can be elongated up to 80% (Fung, 1981; Katoh *et al.*, 1998). Noteworthy, these values of deformation of actin material typically appear in the range of values for initial cable strain used in the viscoelastic-tensegrity model (i.e., $0.05 \leqslant T^* \leqslant 1$).

SCALE EFFECT ON VISCOELASTIC PROPERTIES OF THE CELLULAR-TENSEGRITY MODEL

The present study demonstrates that both structural viscosity and structural elasticity are similarly affected by the structure size, i.e., L^{*-2}-dependency, similar to the scaling law reported for elasticity by previous authors (Wendling *et al.*, 1999, 2000a, b). This property can be used to determine the scaling effects, depending on the size at which cellular mechanical properties are probed. To understand the large scatter of experimental data often reported in living adherent cells concerning the CSK viscosity modulus measured by different techniques, we followed an approach similar to Maksym *et al.* for cellular elasticity (Maksym *et al.*, 2000). We thus attempted to relate typical viscous properties, measured in living adherent cells by different techniques, to the size of probes. Results are plotted in Fig. 9. Although the techniques differed in many other aspects, e.g., loading conditions, type of cells and adhesiveness to the support, we compared in Fig. 9, data

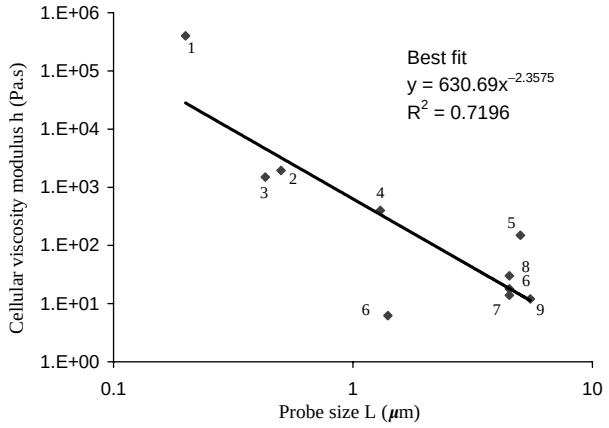

FIG. 9. Experimental cellular viscosity moduli obtained by magnetic techniques, issued from the literature are compared in the same plot. Ragsdale *et al.*[1] (1997) measured cytoplasmic deformation from observations of displacement of fluorescent beads microinjected into the cytoplasm of Swiss 3T3 fibroblasts, in response to tensile stress exerted by centripetal contraction of neighboring cells. Valberg & Albertini[2] (1985), Valberg & Feldman[3] (1987) and Nemoto[4] (1982) used magnetized spherical microbeads that were initially phagocytosed by the tested cells and then mechanically stressed using magnetic tweezers. Laurent *et al.*[5] (2002) used silica beads specifically bound to transmembrane adhesion proteins that are directly related to the actin CSK and then mechanically stressed using optical tweezers. Other authors used ferromagnetic spherical microbeads specifically bound to transmembrane adhesion proteins of the tested cells which were mechanically stressed using magnetic twisting cytometry (step MTC)[6,7,8] (Wang & Ingber, 1994, this study, Wang, 1998) or magnetic oscillatory cytometry (oscillatory MTC) (Maksym *et al.*, 2000)[9].

exclusively obtained with techniques in which probes are specifically attached to the CSK-structure.

Confirming early results reported by Valberg & Albertini (1985), variations in probe size (range: 0.2–5.5 μm) appear to have a predominant effect on cellular viscous measurements which seems to be correlated with the prediction of the tensegrity model characterized by a L^{*-2}-dependence of η^*, with L^* equal to the main characteristic dimension of the CSK-probe (see Fig. 9). It appears that the reported values of viscous modulus in living adherent cells considerably decrease as probe size increases as did elasticity values in Fig. 12 of the recent paper by Maksym *et al.* (2000). Note that the lower cellular viscosity value plotted in Fig. 9 corresponds to magnetic twisting cytometry and could therefore be underestimated for several reasons similar to the one presented to explain the underestimation of E^* in separate papers: (Laurent *et al.*, 2002); Wang, personal communication; (Fabry *et al.*, 1999; Maksym *et al.*, 2000). Results shown in Fig. 9 suggest that the viscoelastic properties of living cells obtained with different techniques could be partly re unified by the tensegrity concept. Since the size parameter cannot summarize the effect of several other factors likely influencing the cellular mechanical response, e.g., CSK-remodeling and cell environment, further studies remain necessary to investigate the whole phenomena influencing the dispersion of experimental data.

In conclusion, the present study supports the mechanical usefulness and biological relevance of the tensegrity concept used to predict the structural origin of cellular viscoelasticity and brings a new confirmation that spatial rearrangement of structural viscoelastic elements constitutes a significant mechanism to understand the CSK mechanical response of living cells. Future cellular models would advantageously incorporate spatial rearrangement as a mechanism capable of explaining and predict the mechanical results in a wide variety of physiological and pathological cellular conditions.

We are indebted to Professors J.J. Fredberg, and N. Wang (Harvard School of Public Health) for helpful discussions.

REFERENCES

ARGYRIS, J. H. & SCHARPF, D. W. (1972). Large deflection analysis of prestressed networks. *J. Struct. Div.* **106,** 633–654.

ARNOLD, V. I. (1973). *Ordinary Differential Equations*. Cambridge, U.S.A., MA, MIT Press.

BEREITER-HAHN, J. & LÜERS, H. (1994). The role of elasticity in the Motile behaviour of cells. In: *Biomechanics of Active Movement and Division of Cells*. (Akkas, N., ed.), Vol. 84, pp. 181–230. Berlin: Springer Verlag.

BRODLAND, G. W. & GORDON, R. (1990). Intermediate filaments may prevent buckling of compressively loaded microtubules. *J. Biomech. Eng.* **112,** 319–321.

BRUHAT, G. (1955). *Mécanique, cours de Physiques Générale*. France, Masson et Cie.

BUTLER, J. P., BIZAL, C. L. & VALBERG, P. A. (1991). Viscoelastic and motile properties of hamster lung and peritoneal macrophages. *J. Leukocyte biol.* **50,** 240–251.

CAILLE, N., THOUMINE, O., TARDY, Y. & MEISTER, J.-J. (2002). Contribution of the nucleus to the mechanical properties of endothelial cells. *J. Biomech.* **35,** 177–187.

Coppel, W. A. (1965). *Stability and Asymptotic Behavior of Differential Equations*. Boston, Heath & Company.

Coughlin, M. F. & Stamenovic, D. (1997). A tensegrity structure with buckling compression elements: application to cell mechanics. *J. Appl. Mech.* **64,** 480–486.

Coughlin, M. F. & Stamenovic, D. (1998). A tensegrity model of the cytoskeleton in spread and round cells. *J. Biomech. Eng.* **120,** 770–777.

Crisfield, M. A., ed. (1991). *Non-linear Finite Element Analysis of Solids and Structures. Essentials*. London: Wiley.

Dennerll, T. J., Buxbaum, R. E. & Heidemann, S. R. (1988). Tension and compression in the cytoskeleton of PC-12 neurites II: quantitative measurements. *J. Cell Biol.* **107,** 664–665.

Elson, E. L. (1988). Cellular mechanism as an indicator of CSK structure and function. *Annu. Rev. Biophys. Biophys. Chem.* **17,** 397–430.

Evans, E. & Yeung, A. (1989). Apparent viscosity and cortical tension of blood granulocytes determined by micropipet aspiration. *Biophys. J.* **56,** 151–160.

Fabry, B., Maksym, G. N., Hubmayr, R. D., Butler, J. P. & Fredberg, J. J. (1999). Implications of heterogeneous bead behavior on cell mechanical properties measured with magnetic twisting cytometry. *J. Magn. Magn. Mater.* 19**4,** 120–125.

Fabry, B., Maksym, G. N., Butler, J. P., Glogauer, M., Najavas, D. & Fredberg, J. J. (2001). Scaling the microrheology of living cells. *Phys. Rev. Lett.* **87,** 14 8102-1;14 8102-4.

Fredberg, J. J. & Stamenovic, D. (1989). On the imperfect elasticity of lung tissue. *J. Appl. Physiol.* **67,** 2408–2419.

Fung, Y. C., Ed. (1981). *Biomechanics; Mechanical Properties of Living Tissues*. University of California, San Diego: Springer-Verlag.

Fung, Y. C. & Liu, S. Q. (1993). Elementary mechanics of the endothelium of blood vessels. *J. Biomech. Eng.* **115,** 1–12.

Gantmacher, F. R. (1966). *Théorie des Matrices*. Tomes 1 & 2. Paris: Dunod.

Heidemann, S. R. & Buxbaum, R. E. (1990). Tension as a regulator and integrator of axonal growth. *Cell Motility Cytoskeleton* **17,** 6–10.

Heidemann, S. R., Kaech, S., Buxbaum, R. E. & Matus, A. (1999). Direct observations of the mechanical behaviors of the cytoskeleton in living fibroblasts. *J. Cell Biol.* **145,** 109–122.

Hochmuth, R. M. & Waugh, R. E. (1987). Erythrocyte membrane, elasticity and viscosity. *Annu. Rev. Physiol.* **49,** 209–219.

Ingber, D. (1993). Cellular tensegrity: defining new rules of biological design that govern the cytoskeleton. *J. Cell Sci.* **104,** 613–627.

Ingber, D. E. (1997). Tensegrity: the architectural basis of cellular mechanotransduction. *Annu. Rev. Physiol.* **59,** 575–599.

Ingber, D. E. (1998). Tensegrity and the emergence of a cellular biophysics. In: *Dynamical Networks in Physics and Biology* (Beysens, D. & Forgacs, G., eds.), Vol. 10. Berlin: EDP Sciences, Springer-Verlag.

Ingber, D. & Folkman, J. (1989). Tension and compression as basic determinants of cell form and function: utilization of a cellular tensegrity mechanism. In: *Cell Shape: Determinants, Regulation and Regulatory Role* (S. W. D. & B. F., eds.), Vol. 1. pp. 3–31. Academic press Inc.

Ingber, D. E. & Jamieson, J. D. (1985). Cells as tensegrity structures: architectural regulation of histodifferentiation by physical forces transduced over basement membrane. In: *Gene Expression During Normal and Malignant Differentiation*. Anderson, L., Gahmberg, C. & Ekblom, P., eds.), pp. 13–32. London: San Diego Academic Press.

Ingber, D. E. & Karp, S. (1991). Control of cell and nuclear form through establishment of tensional integrity between cytoskeletal struts and extracellular matrix anchors. *J. Cell Biol.* **115,** 394A.

Ingber, D. E., Dike, L., Sims, J. & Hansen, L. (1994). Cellular tensegrity: exploring how mechanical changes in the cytoskeleton regulate cell growth, migration and tissue pattern during morphogenesis.

Ingber, D. E., Prusty, D., Sun, Z., Betensky, H. & Wang, N. (1995). Cell shape, cytoskeleton mechanics and cell cycle control in angiogenesis. *J. Biomech.* **28,** 1471–1484.

Ingber, D. E., Heidemann, S. R., Lamoureux, P. & Buxbaum, R. E. (2000). Opposing views on tensegrity as a structural framework for understanding cell mechanics. *J. Appl. Physiol.* **89,** 1663–1678.

Janmey, P. A. & Stossel, T. P. (1988). Viscoelasticity of F-actin and F-Actin/gelsolin complexes. *Biochemistry* **27,** 8218–8226.

Janmey, P. A., Hvidt, S., Ferry, J. D. & Stossel, T. P. (1989). Actin filaments as a model for rigid polymer networks. In: *Physical Networks, Polymers and Gels* (Ross-Murphy, W. B. A. S., ed.), pp. 359–369. London & New York: Elsevier Applied Science.

Janmey, P. A., Euteneuer, U., Traub, P. & Schliwa, M. (1991). Viscoelastic properties of vimentin compared with other filamentous biopolymer networks. *J. Cell Biol.* **113,** 155–160.

Katoh, K., Kano, Y., Masuda, M., Onishi, H. & Fujiwara, K. (1998). Isolation and contraction of the stress fibers. *Mol. Biol. Cell* **9,** 1919–1938.

Kebiche, K., Kazi-Aaoual, M. N. & Motro, R. (1999). Geometrical nonlinear analysis of tensegrity systems. *Eng. Struct.* **21,** 864–876.

Kojima, H., Ishijima, A. & Yanagida, T. (1994). Direct measurement of stiffness of single actin filaments with and without tropomyosin by in vitro nanomanipulation. *Proc. Natl Acad. U.S.A.* **91,** 12 962–12 966.

Laurent, V. M., Henon, S., Planus, E., Fodil, R., Balland, M., Isabey, D. & Gallet, F. (2002). Assessment of mechanical properties of adherent living cells by bead micromanipulation: comparison of magnetic twisting cytometry vs optical tweezers. *J. Biomech. Eng.* (in press).

Maksym, G. N., Fabry, B., Butler, J. P., Navajas, D., Tschumperlin, D. J., Laporte, J. D. & Fredberg, J. J. (2000). Mechanical properties of cultured human airway smooth muscle cells from 0.05 to 0.4 Hz. *J. Appl. Physiol.* **89,** 1619–1632.

Mathur, A. B., Truskey, G. A. & Reichert, W. M. (2000). Atomic force and total reflection fluorescence microscopy for the study of force transmission in endothelial cells. *Biophys. J.* **78,** 1725–1735.

Mohri, F. & Motro, R. (1993). Static and kinematic determination of generalized space reticulated systems. *Struct. Eng. Rev.* **5,** 231–237.
Nemoto, I. (1982). A model of magnetization and relaxation of ferrimagnetic particles in the lung. I.E.E.E. (*Institute of Electrical and Electronics Engineers*) *Trans. Biomed. Eng.* **29,** 745–752.
Planus, E., Galiacy, S., Matthay, M., Laurent, V., Gavrilovic, J., Murphy, G., Clerici, C., Isabey, D., Lafuma, C. & D'Ortho, M. P. (1998). Role of collagenase in mediating in vitro alveolar epithelial wound repair. *J. Cell Sci.* **112,** 243–252.
Pugh, A., Ed. (1976). *Introduction to Tensegrity*. California: University of California Press.
Ragsdale, G. K., Phelps, J. & Luby-Phelps, K. (1997). Viscoelastic response of fibroblasts to tension transmitted through adherens junctions. *Biophys. J.* **73,** 2798–2808.
Satcher, R. L. & Dewey, C. F. (1996). Theoretical estimates of mechanical properties of the endothelial cell cytoskeleton. *Biophys. J.* **71,** 109–118.
Sato, M., Theret, D. P., Wheeler, L. T., Ohshima, N. & Nerem, R. M. (1990). Application of the micropipette technique to the measurement of cultured porcine aortic endothelial cell viscoelastic properties. *J. Biomech. Eng.* **112,** 263–268.
Stamenovic, D. & Coughlin, M. F. (1999). The role of prestress and architecture of the cytoskeleton and deformability of cytoskeletal in mechanics of adherent cells: a quantitative analysis. *J. theor. Biol.* **201,** 63–74.
Stamenovic, D. & Coughlin, M. F. (2000). A quantitative model of cellular elasticity based on tensegrity. *J. Biomech. Eng.* **122,** 39–43.
Stamenovic, D. & Wang, N. (2000). Engineering approaches to cytoskeletal mechanics. *J. Appl. Physiol.* **89,** 2085–2090.
Stamenovic, D., Ingber, D. E., Wang, N. & Fredberg, J. J. (1996). A microstructural approach to cytoskeletal mechanics based on tensegrity. *J. theor. Biol.* **181,** 125–136.
Stamenovic, D., Liang, Z., Chen, J. & Wang, N. (2002). Effect of the cytoskeletal prestress on the mechanical impedance of cultured airway smooth muscle cells. *J. Appl. Physiol.* **92,** 1443–1450.
Thoumine, O. & Ott, A. (1997). Time scale dependent viscoelastic and contractile regimes in fibroblasts probed by microplate manipulation. *J. Cell Sci.* **110,** 2109–2116.
Valberg, P. A. & Albertini, D. F. (1985). Cytoplasmic motions, rheology and structure probed by a novel magnetic particle method. *J. Cell Biol.* **101,** 130–140.
Valberg, P. A. & Feldman, H. A. (1987). Magnetic particle motions with living cells (measurement of cytoplasmic viscosity and motile activity). *Biophys. J.* **52,** 551–561.
Volokh, K. Y., Vilnay, O. & Belsky, M. (2000). Tensegrity architecture explains linear stiffening and predicts softening of living cells. *J. Biomech.* **33,** 1543–1549.
Wang, N. (1998). Mechanical interactions among cytoskeletal filaments. *Hypertension* **32,** 162–165.
Wang, N. & Ingber, D. E. (1994). Control of cytoskeletal mechanics by extracellular matrix, cell shape and mechanical tension. *Biophys. J.* **66,** 1–9.
Wang, N., Naruse, K., Stamenovic, D., Fredberg, J. J., Mijailovich, S. M., Tolic-Norrelykke, I. M., Polte, T., Mannix, R. & Ingber, D. E. (2001). Mechanical behavior in living cells consistent with the tensegrity model. *Proc. Natl Acad. Sci. U.S.A.* **98,** 7765–7770.
Wang, N., Tolic-Norrelykke, I. M., Chen, J., Mijailovich, S., Butler, J. P., Fredberg, J. J. & Stamenovic, D. (2002). Cell prestress. I. Stiffness and prestress are closely associated in adherent contractile cells. *Am. J. Physiol. Cell Physiol.* **282,** C606-C616.
Wendling, S., Oddou, C. & Isabey, D. (1999). Stiffening response of a cellular tensegrity model. *J. theor. Biol.* 19**6,** 309–325.
Wendling, S., Planus, E., Laurent, V. M., Barbe, L., Mary, A., Oddou, C. & Isabey, D. (2000a). Role of cellular tone and microenvironmental conditions on cytoskeleton stiffness assessed by tensegrity model. *Eur. Phys. J. AP* **9**, 51–62.
Wendling, S., Oddou, C. & Isabey, D. (2000b). Approche structurale de la mécanique du cytosquelette : solide alvéolaire vs modèle de tenségrité. *Compte Rendu de l'Académie des Sciences. Paris* **t. 328** (Sér. II b; Biomécanique), 97–104.
Yamada, S., Wirtz, D. & Kuo, S. C. (2000). Mechanics of living cells measured by laser tracking microrheology. *Biophys. J.* **78,** 1736–1747.

APPENDIX

The constitutive law of an elastic isotropic medium is given by the following equation:

$$\sigma = \lambda \,\mathrm{Tr}(\varepsilon)1 + 2\mu\varepsilon, \tag{A.1}$$

where $\boldsymbol{\sigma}$ is the stress tensor, $\boldsymbol{\varepsilon}$ is the resulting strain tensor, $\mathbf{1}$ is the identity tensor and $\boldsymbol{\lambda}$ and $\boldsymbol{\mu}$ are, respectively, the first and second Lame coefficients, which are related to the Young and shear moduli by classical relations shown below:

$$\mu \equiv G = \frac{E}{2(1+\nu)}. \tag{A.2}$$

In the case of isotropic elasticity, one may write:

$$E = \frac{\sigma_{11}}{\varepsilon_{11}}, \tag{A.3}$$

$$\nu = -\frac{\varepsilon_{22}}{\varepsilon_{11}}, \tag{A.4}$$

where subscript 1 and 2 refer to the longitudinal and transverse directions in the studied medium, respectively.

Equation (A.4) indicates that during extension, as length of a given sample of the medium increases, transverse dimension decreases, leading to a positive Poisson's ratio. Note that a negative Poisson's ratio would correspond to an increase in the sample thickness whereas sample length increases.

Furthermore, for an isotropic elastic continuous medium (whose constitutive laws derive from a quadratic potential), v obeys the following conditions:

$$-1 < v < \tfrac{1}{2}. \tag{A.5}$$

If the Poisson ratio happens to be greater than 0.5, the studied material is not an isotropic continuous medium.

The present values of v obtained for the tensegrity model (summarized in Table 2) do not obviously correspond to an elastic isotropic continuous medium, consistently with the discrete nature of the structure. Incidentally, the present values of the global Poisson's ratio differ from those obtained in a previous study on a similar tensegrity structure (Stamenovic & Coughlin, 1999). This result is not surprising because both nodal attachment and type of loading in the latter study completely differed from the present study: Stamenovic and Coughlin do not attach the tensegrity structure to a substratum, but simulate a stretching effort which consists in pulling apart two parallel bars which results in an inflation of the global tensegrity structure evidenced by the higher spacing between parallel free bars, hence the negative values of v was found, as explained above. By contrast, the extension mode and attachment conditions used in the present study do not result in such an inflation of the structure, hence the positive values of v presently found.